Supplemental information

Perfluorinated alkyl groups induce unexpected hydrophobic hydration structure

Simon Schulke[†] [a], Elio Casalini[†] [b], Jaspreet Kaur[a], Sulejman Skoko[b], Gerhard Schwaab[a], Martina Havenith[a,*], Ana Vila Verde[b,*].

[a] Ruhr-University Bochum, Faculty for Chemistry and Biochemistry, Universitätsstraße 150, 44801 Bochum

[b] University of Duisburg-Essen, Faculty of Physics, Lotharstr. 1, 47057 Duisburg, Germany

[†] These authors contributed equally to this work. [*] Corresponding authors: Martina Havenith, Martina.Havenith@ruhr-uni-bochum.de; Ana Vila Verde, ana.araujo-vila-verde@uni-due.de.

S1 Experimental SI

S1.1 Data processing

We determine the absorption coefficient of our sample by measuring the difference in absorption coefficients ($\Delta\alpha$) between the sample and a reference, here bulk water.

$$\ln\left(\frac{I_0(\tilde{\nu})}{I_s(\tilde{\nu})}\right)\cdot\frac{1}{d}=\alpha_s(\tilde{\nu})-\alpha_0(\tilde{\nu})=\Delta\alpha(\tilde{\nu}) \tag{S1}$$

Here, $I_0(\tilde{\nu})$ refers to the frequency dependent transmitted light intensity of the reference and $I_s(\tilde{\nu})$ to the frequency dependent transmitted light intensity of the sample. $\alpha_s(\tilde{\nu})$ and $\alpha_0(\tilde{\nu})$ correspond to the frequency dependent absorption coefficients of the sample and reference, respectively. Using the Fabry-Perot etalon effect, we can calculate the thickness of the sample (d) by measuring the interference pattern of the empty sample cell[1]. We chose water as our reference to reduce the errors introduced by the significant difference in the refractive indices of the air and the sample. By adding the known frequency dependent absorption coefficient of bulk water to the difference in (S1), we obtain the frequency dependent absorption coefficient of our sample.

$$\alpha_s(\tilde{\nu})=\Delta\alpha(\tilde{\nu})+\alpha_0(\tilde{\nu}) \tag{S2}$$

Dividing the calculated absorption coefficient of our sample in equation S2 by the total concentration of substances in the sample volume (c_s), we obtain the frequency dependent molar extinction coefficient ($\varepsilon_s(\tilde{\nu})$):

$$\varepsilon_s(\tilde{\nu})=\frac{\alpha_s(\tilde{\nu})}{c_s} \tag{S3}$$

Lastly, by subtracting the mole-fraction weighted (x_i) frequency dependent molar extinction coefficients of the bulk substances ($\varepsilon_i^{bulk}(\tilde{\nu})$), we obtain the frequency dependent excess molar extinction coefficient ($\varepsilon^E(\tilde{\nu})$):

$$\varepsilon^E(\tilde{\nu})=\varepsilon_s(\tilde{\nu})-\sum_i x_i\cdot\varepsilon_i^{bulk}(\tilde{\nu}) \tag{S4}$$

The molar extinction coefficients of bulk liquid 2,2,2-trifluoroethanol (TFE) and ethanol (EtOH) were obtained by measuring the pure liquids at different sample thicknesses d_1 and d_2 and referencing the result to the bulk concentration of TFE or EtOH (c_i^{bulk}):

$$\ln\left(\frac{I_1(\tilde{\nu})}{I_2(\tilde{\nu})}\right)\cdot\frac{1}{d_2-d_1}\cdot\frac{1}{c_i^{bulk}}=\varepsilon_i^{bulk}(\tilde{\nu}) \tag{S5}$$

The absorption coefficient and molar extinction coefficient of bulk water are obtained by fitting complex valued damped harmonic oscillators to different datasets from the literature and our own measurements, including attenuated total reflectance (ATR), transmission and dielectric measurements of water in the THz frequency range.

In order to remove interference fringes from our spectra, caused by back-reflections in the diamond windows of our sample cell, we performed a simple correction according to the method presented by Neri *et al.*.

S1.2 Molar extinction and excess molar extinction coefficients

In the following we present the molar extinction and excess molar extinction coefficients for EtOH and TFE for all measured concentrations. The sharp feature in the EtOH spectra at 432 cm^{-1} in Fig. S1 (i) can

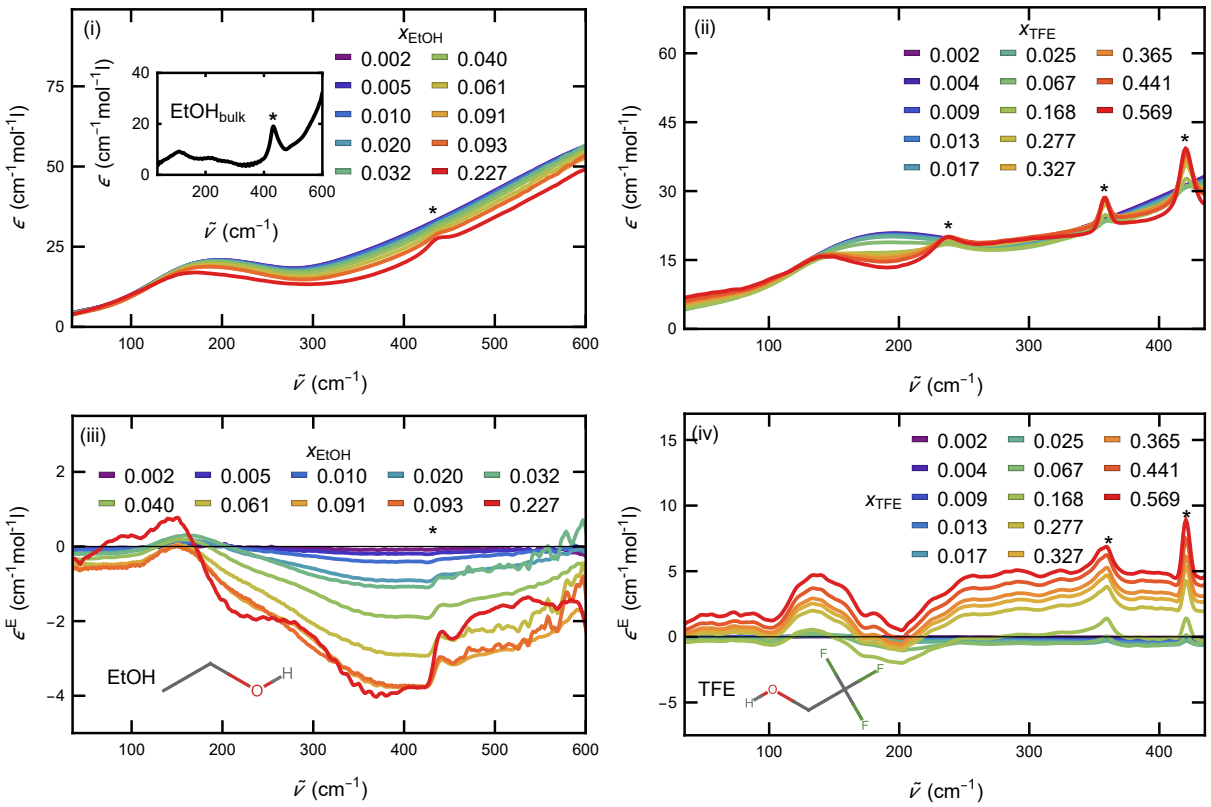

Fig. S1 (i) Molar extinction coefficients of aqueous EtOH solutions with mole-fractions of EtOH ranging from 0.002 to 0.227, at 20 °C. (ii) Molar extinction coefficients of aqueous TFE solutions with mole-fractions of TFE ranging from 0.002 to 0.569, at 20 °C. (iii) Excess molar extinction coefficients of aqueous EtOH solutions with mole-fractions of ethanol ranging from 0.002 to 0.227, at 20 °C. (iv) Excess molar extinction coefficients of aqueous TFE solutions with mole-fractions of TFE ranging from 0.002 to 0.569, at 20 °C. The inset in (i) shows the molar extinction coefficient of bulk EtOH at 20 °C. The asterisks mark intramolecular absorption modes of the alcohols.

be assigned to an intramolecular ethanol vibration from IR and Raman measurements[3]. This absorption mode undergoes a frequency shift depending on the composition of the water-EtOH mixture, which is the cause for the sharp feature at the corresponding frequency in the excess molar extinction coefficient spectra in panel (iii) of Fig. S1. Due to excessive noise in some of the EtOH spectra beyond 425 cm^{-1} we excluded this frequency range from the principal component analysis. For the same reason, we excluded data for TFE beyond 435 cm^{-1}.

S1.3 Principal Component analysis

For the analysis of the mole-fraction dependent alcohol spectra we performed a principal component analysis (PCA) of $\varepsilon^E(\tilde{\nu})$ to identify their main spectroscopic components[4]. We confined the PCA to the frequency region of 30 cm^{-1} to 435 cm^{-1} for TFE and to 30 cm^{-1} to 415 cm^{-1} for EtOH due to excessive noise in the spectra beyond these ranges. The spectral dissection is based on a singular value decomposition (SVD) of a matrix **Data** containing the excess molar extinction coefficients of all measurements as row vectors. The SVD returns three matrices: the **S** matrix is orthonormal to the **Data** Matrix and contains the weights for each principal component as row vectors, the **SV** matrix (diagonal) contains the singular

values and the **L** matrix, also orthonormal, contains the eigenvectors for each principal component and describes the data as column vectors. The original **Data** matrix can be fully reconstructed by[4]:

$$\mathbf{Data} = \mathbf{S} \times \mathbf{SV} \times \mathbf{L}^{\mathrm{T}} \tag{S6}$$

The columns of **S** contain the mole-fraction dependent information for each spectral component (also called "Scores") and the columns of **L** contain the spectral information (also called "Loadings"). For further discussion, we will refer to a principal component as the product of a column of the matrix **L** (eigenvectors describing the spectral information) with its corresponding singular value **SV**. The first principal component is akin to the spectral average over the range covered by the observed variable, here the mole-fraction of the alcohol, whereas successive principal components describe deviations from this average. The highest order principal components usually contain mainly small statistical and systematic errors. This approach allows us to distinguish between physically meaningful spectral components and noise.

The first five principal components of the EtOH excess molar extinction spectra are shown together with their weights (**S** matrix) in Fig S2. Looking at the Loadings values in Fig. S2 shows that the first 3 components mainly contribute to the information in the spectra. This fact becomes more clear if the Scores are taken into consideration as well. Here, beyond the third component, the Scores show a random behavior with mole-fraction, indicating, that these components only describe statistical errors in our measurements.

The first five main components of the TFE excess molar extinction spectra are shown together with their weights (**S** matrix) in Fig S3 Looking at the Loadings values in Fig. S3 shows that also for TFE the first 3 components mainly contribute to the information in the spectra. Just like for EtOH, this fact becomes more clear if the Scores are taken into consideration as well. Again, a random behavior with mole-fraction can be seen for the higher order principal components. This random behavior can again be attributed to statistical errors in our measurements.

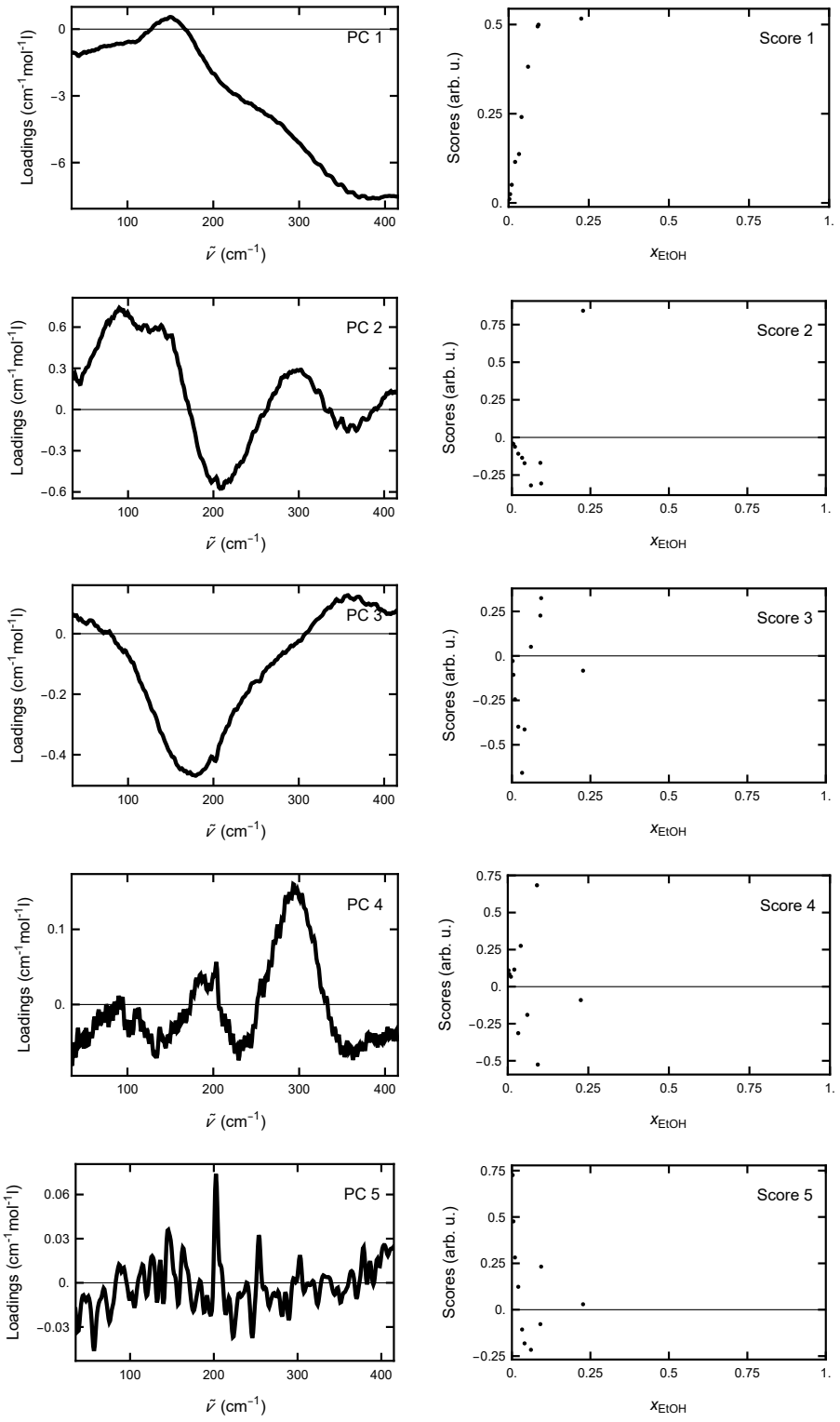

Fig. S2 First five principal components of the excess molar extinction coefficient of EtOH. The frequency range for the principal component analysis is reduced to 30 cm^{-1} to 415 cm^{-1} due to excessive noise beyond that range. The first 3 principal components mainly contribute to the spectra.

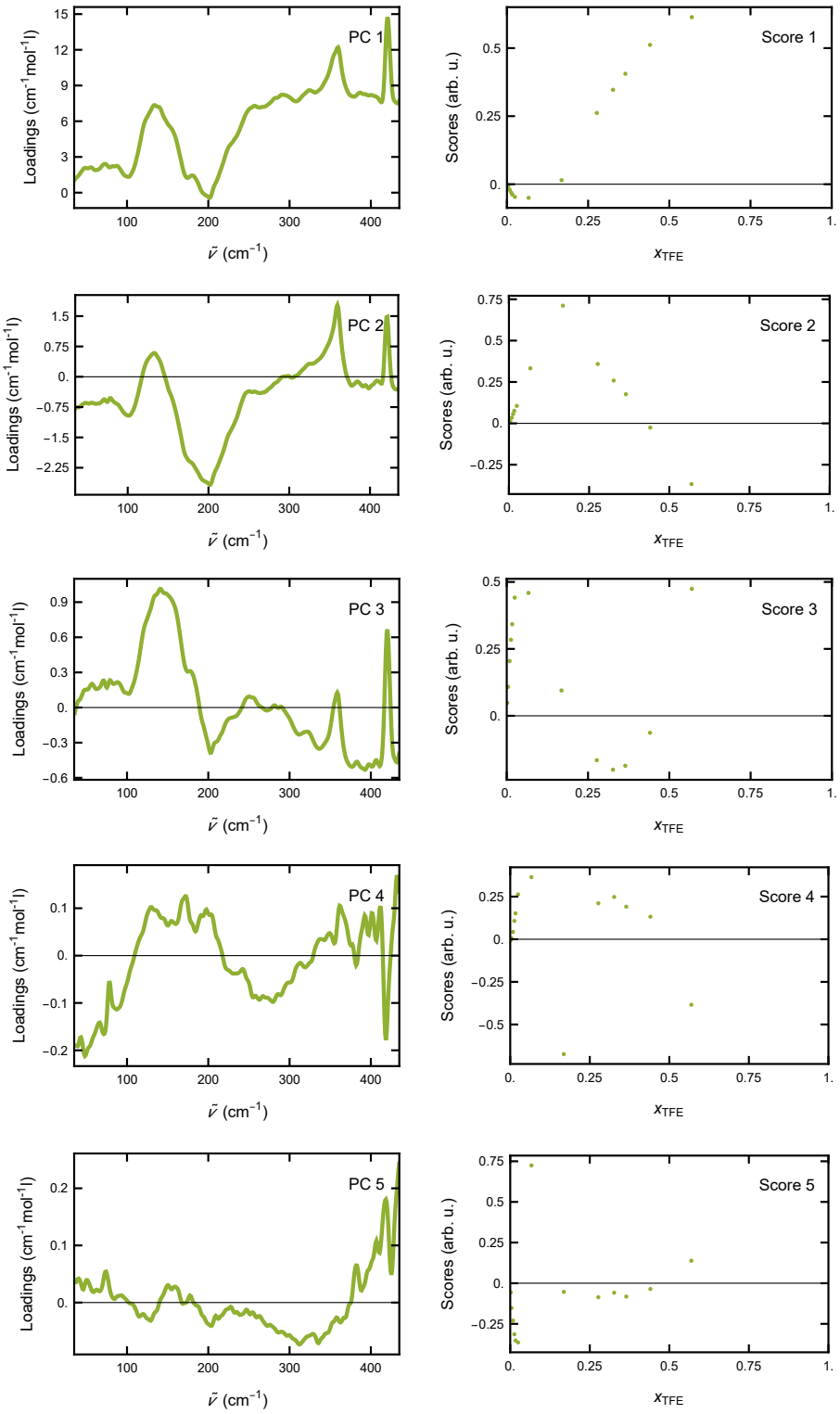

Fig. S3 First five principal components of the excess molar extinction coefficient of TFE. The frequency range for the principal component analysis is reduced to 30 cm^{-1} to 435 cm^{-1} due to excessive noise beyond that range. The first 3 principal components mainly contribute to the spectra.

S2 Computational SI

S2.1 Ab Initio Molecular Dynamics and THz spectra

To reliably predict THz spectra, it is essential to obtain an accurate thermodynamic and structural description of the solvation shell. Standard density functionals are known to over-structure liquid water, yielding a hydrogen-bond network that is excessively rigid compared to experiment[5–7]. In the case of ethanol (EtOH) and 2,2,2-trifluoroethanol (TFE), this limitation leads to an overestimation of the population of strong solvent hydrogen bonds and to an underestimation of dangling OH groups (hydroxy groups not donating hydrogen bonds), which play a key role in shaping the solvation environment — particularly for TFE[8]. Previous studies attempted to alleviate this problem by artificially raising the equilibration temperature[9,10]; however, this approach substantially perturbs water dynamics, distorts the THz spectral region, and ultimately serves as a workaround rather than a rigorous solution. More recently, the revPBE functional has demonstrated to reproduce the oxygen–oxygen radial distribution function of liquid water with high fidelity[11]. For this reason, revPBE was employed in the AIMD-DFT simulations reported in this work.

S2.2 Water vibrational spectra

To verify that the simulations proceeded correctly and without anomalies, the IR and THz spectra of bulk water were calculated and compared with previously reported literature data[9,10]. Spectra in Fig.S4

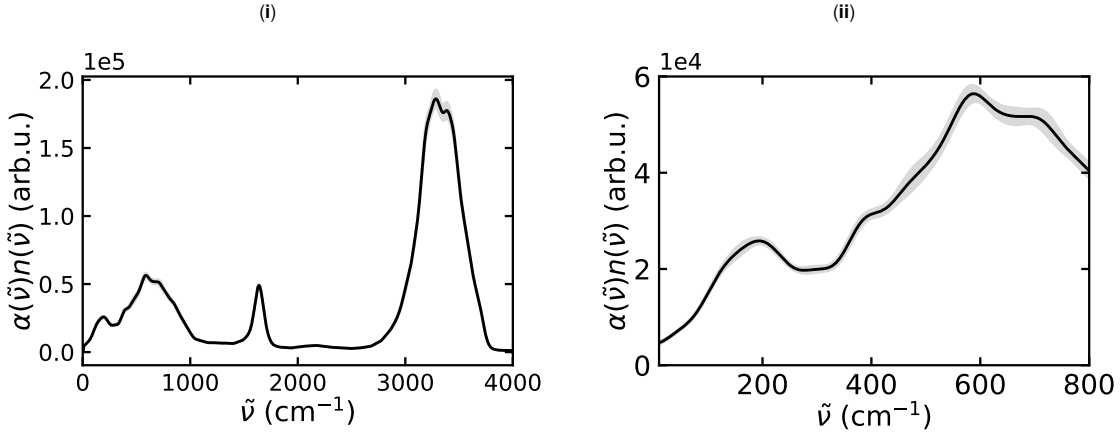

Fig. S4 Computed spectra for the (i) full IR range and (ii) THz region for bulk water. The SEM is shown as the shadowed region.

shows good agreement with the spectra reported in literature. In the THz region, our spectrum displays a weaker peak around 200 cm^{-1} and a more intense peak near 600 cm^{-1}. IR spectra also exhibits a sharp single peak at approximately 1600 cm^{-1} and a broad band centered around 3000 cm^{-1}, corresponding to hydrogen-bonded water molecules. The only noticeable difference is that in the reference spectrum the hydrogen-bonded band extends to lower wavenumber (starting at 2600 cm^{-1}). This behavior is fully consistent with expectations, as the reference employed the PBE functional, which is well known to over-structure the hydrogen-bond network in liquid water, thereby enhancing contributions in the region associated with strong hydrogen bonding.

S2.3 Probability density histograms from quantum mechanics

After confirming that the bulk water vibrational spectra obtained from Ab Initio Molecular Dynamics (AIMD) are consistent with both experimental and previously reported computational results—thereby providing a solid validation of the Density Functional Theory (DFT) approach—it becomes necessary to establish a further connection between the AIMD methodology and Classical Molecular Dynamics (CMD). To this end, probability density distribution histograms were computed and plotted for AIMD simulations of TFE, EtOH, and bulk water, along with their relative differences, and subsequently compared with

those reported in the main text, showed in Fig.7.

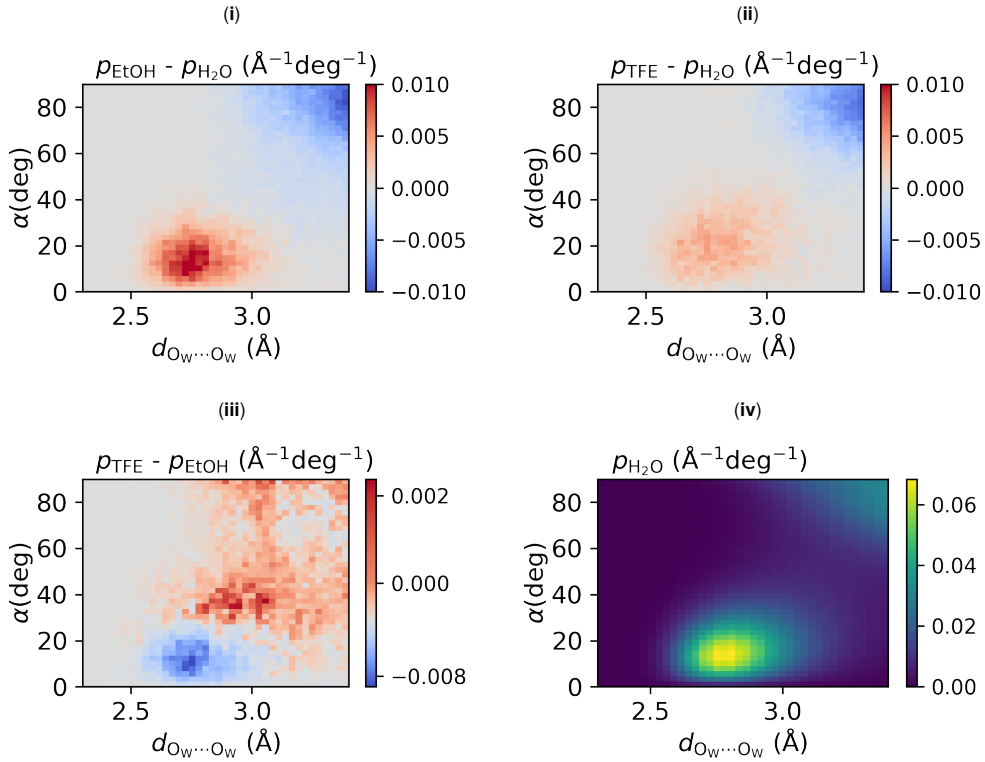

Fig. S5 Differences in AIMD probability density of water–water spatial distributions between: (i) the water shell surrounding the methyl group of EtOH and water in the bulk,(ii) the water shell surrounding the perfluoromethyl group of TFE and water in the bulk, and (iii) the water shell surrounding the perfluoromethyl group of TFE and the water shell surrounding the methyl group of EtOH. Red regions indicate larger $p_s(d,\alpha)$ for the first species in each pair, while blue regions indicate larger $p_s(d,\alpha)$ for the second. In (iv) the absolute AIMD probability density distribution for bulk water is reported.

These plots show very good agreement with the Classical Molecular Dynamics (CMD) results (reported in Fig. 7). Both solutes perturb the hydrogen-bond network of bulk water, enhancing the overall probability of hydrogen bonding. Ethanol leads to a greater increase in the probability of strong hydrogen bonds, whereas TFE promotes hydrogen bonding over a broader angular range. A direct comparison between the two solutes highlights a clear difference in the population between 25° and 50°. Given the agreement between AIMD and CMD, as well as the consistency between AIMD and the experimental THz spectra, we can conclude that both methods provide a reliable description of the solvation shell around these solutes. Owing to the significantly lower computational cost of CMD, the subsequent analysis of the solvation shells is therefore carried out using CMD simulations.

S2.4 Dissecting CMD Histograms

Because of the very different chemical nature of the groups in our solutes, we dissected the probability density of the water-water distribution perturbations according to the different classes of hydrogen bonds formed. Specifically, we considered: hydrogen bonds involving the solute hydroxy group, which can act as both donor and acceptor; hydrogen bonds between water molecules within the first solvation shell; and hydrogen bonds between a water molecule inside the first solvation shell (acting as either donor or acceptor) and a water molecule outside this shell. The histograms in Fig. S6 show that outer-inner and inner-outer water hydrogen bonds are essentially identical for TFE and EtOH, and mostly noise driven, whereas both inner-inner water hydrogen bonds and those involving water as a donor to the alcohol are more probable to be found in the hydrogen-bond region for EtOH compared to TFE. Water-Alcohol probability density histograms are not different from the pure counting of these HB distributions reported in the main document (Fig. 8 (ii) and (iii)) because the interactions between the alcohol group and water

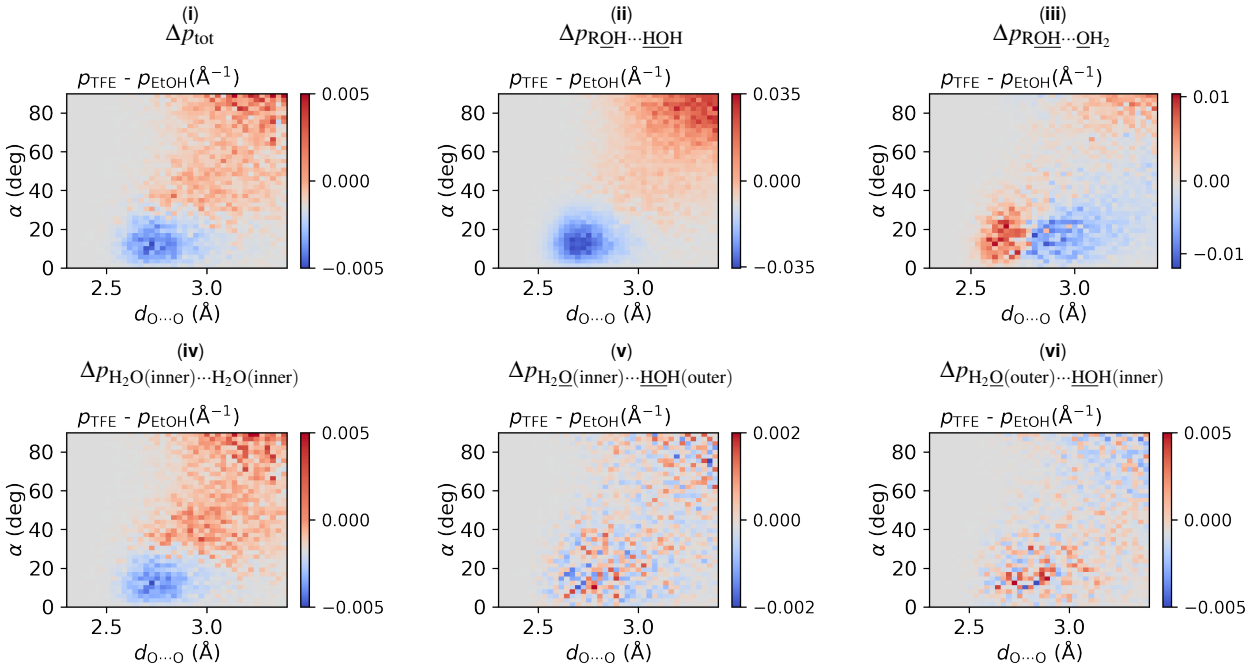

Fig. S6 Probability density differences of TFE and EtOH for the spatial distributions of (i) all the possible kind of OH, (ii) water OH relatively to the alcoholic O of the solutes, (iii) alcohol OH group to the water oxygen, (iv) water - water within the solvation shell cutoff, (v) water oxygen within the solvation shell cutoff and water OH beyond this cutoff, (vi) water OH within the solvation shell cutoff and a water O beyond this cutoff.

are independent from the size of the solvation shell surrounding CF_3 or CH_3. An additional noteworthy feature appears in Fig. S6(iii), where alcohol donating a hydrogen bond to water is more likely at larger distances for TFE than for EtOH.

S2.5 Counting perturbed HB

The perturbation of the HB network induced by each solute was quantified as described in the main text in Fig. 8. Hydrogen bonds were identified by selecting histogram regions corresponding to angles below 45° and donor to acceptor distances shorter than 3.2 Å. Each interaction within this range was counted as one HB per solute. To assess the relative perturbation introduced by the two solutes, the number of hydrogen bonds perturbed by EtOH was subtracted from those perturbed by TFE, thereby providing a direct measure of their different effect on the water network. In Fig. S7, the contributions from inner

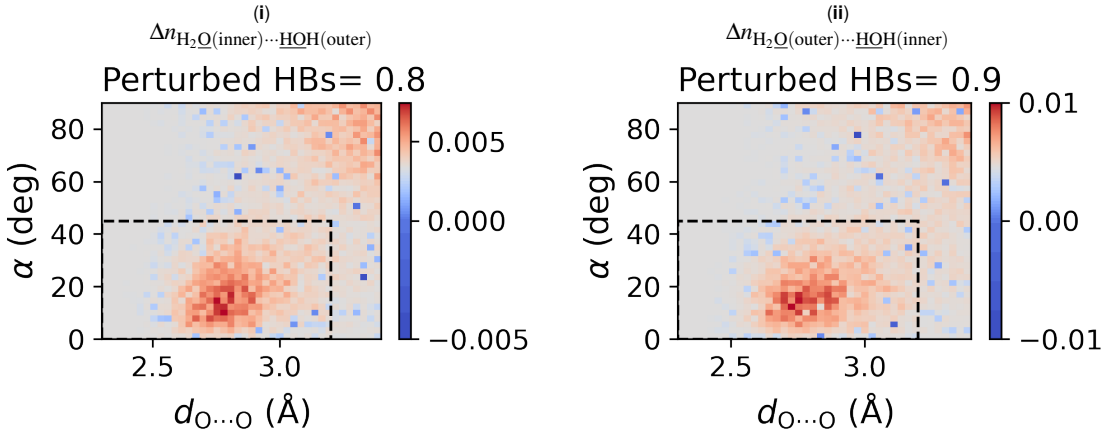

Fig. S7 Number of perturbed OH groups differences between TFE and EtOH for (i) water oxygen acceptor in the first solvation shell and water OH beyond the solvation shell cutoff, (ii) water OH within the first solvation shell as donor, and water oxygen acceptor beyond the solvation shell.

to outer and outer to inner hydrogen bonds are also reported. The corresponding color scales appear

comparable to those obtained for alcohol-water interactions. However, while alcohol-water interactions are limited to a maximum of two hydrogen bonds per solute, interactions between the first (inner) and second (outer) solvation shells can involve a much larger number of water molecules. Since these histograms are based on raw counts, the observed differences in solvation-shell perturbations between TFE and EtOH are extremely small, likely negligible, and primarily arising from the larger solvation shell of TFE compared to EtOH, as showed in S2.6

S2.6 Radial distribution functions

Radial distribution functions were computed for the oxygen atoms of water, using the methyl and perfluoromethyl carbon atoms of EtOH and TFE, respectively, as reference points. Results depicted in Fig. S8

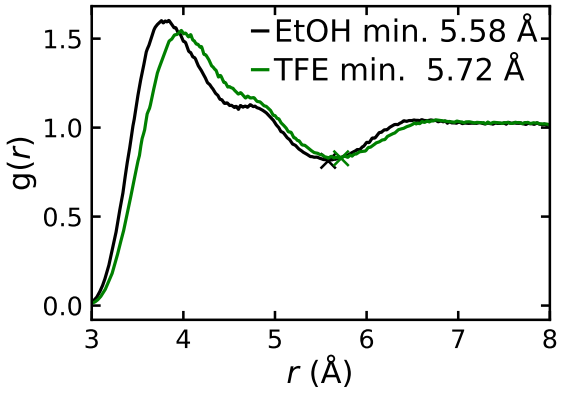

Fig. S8 Radial distribution functions of water O from methyl C of the EtOH in black and perfluoromethyl C of TFE in green. The crosses indicate the minimum of each curve.

reveal distinct qualitative differences in the radial distribution functions of the two solutes. Specifically, the TFE distribution is characterized by a shift of both its primary maximum and global minimum to larger distances, indicating a bigger solvation shell. Furthermore, the reduced intensity of both the maximum and minimum for TFE, when compared to EtOH, suggests a less pronounced ordering of the surrounding water molecules, in agreement with the probability density distribution showed in Fig. 7. Furthermore, a notable difference is observed in the secondary peak of hydration shell, located at approximately 5 Å. The band corresponding to this shell is significantly sharper for EtOH, while for TFE it is broader and largely absorbed into the primary peak. This difference suggests that the solvation shell is less structured around TFE.

S2.7 Random Network Model

S2.7.1 Input values

The observables in Table 1 in the main text were scaled to minimize force-field dependency, following the procedure described by Madan and coworkers[12]:

$$z_{11,\mathrm{n}} = Z_0 + Z_0\left(\frac{z_{11} - z_0}{z_0}\right) \tag{S7}$$

Here Z_0 denotes values for one of $\overline{R}$, $\overline{\delta R^2}$ or $\overline{\alpha^2}$, as reported in the original RNM study[13]and z_{11} or z_0 refer to the values of the same property obtained from our simulations (Table 1); the subscript "0" indicates the observable is for water in the bulk, the subscript "11" indicates it was calculated considering only the first solvation shell of the solute and the subscript "n" denotes the new, scaled quantity, obtained from these values. This scaling approach has been applied in other RNM studies of thermodynamics of hydration of nonpolar solutes[14]. The scaled values are shown in Table S1 and were used as input in the RNM to calculate the entropy and enthalpy of bulk water and of the solvation-shell water around the two

solutes[13,15].

system	$\overline{R_s}$ (Å)	$(\overline{\delta R_s^2})^{1/2}$ (Å)	$(\overline{\alpha_s^2})^{1/2}$ (deg)
bulk	2.848	0.063	15.65
EtOH	2.843	0.063	15.41
TFE	2.847	0.063	15.58

Table S1 Scaled $\overline{R_s}$, $(\overline{\delta R_s^2})^{1/2}$ and $(\overline{\alpha_s^2})^{1/2}$ for water in the first solvation shell of the indicated solutes, obtained from the values in Table 1 through eq. S7, and for water in the bulk (from ref. 13), used as input for the Random Network Model. The scaled values have associated statistical uncertainty in the last significant digit or lower. They are listed with the same number of significant digits as the reference values, for which the statistical uncertainty was not reported.

S2.7.2 RNM dissected results

The thermodynamics of solvation of the two solutes, dissected by each contribution to the total property, are are presented in Tables S2 and S3. The first three terms of both tables refer to the lattice librational,

Table S2 Contributions to the entropy of solvation for TFE, EtOH and difference of these contributions for the two solutes.

Description	TFE (J/(K mol))	EtOH (J/(K mol))	EtOH - TFE (J/(K mol))
$\Delta S_{vib}^{libr}\left(\overline{\alpha_s^2}\right)$	-0.67	-1.96	-1.29
$\Delta S_{vib}^{tras}\left(\overline{\alpha_s^2}\right)$	-0.72	-2.13	-1.41
$\Delta S_{vib}^{bend}\left(\overline{\alpha_s^2}\right)$	-0.38	-1.11	-0.73
ΔS_p	0.00	0.00	0.00
$\Delta S_R(\overline{\delta R_s^2})$	0.00	0.00	0.00
$\Delta S_B\left(\overline{\alpha_s^2}\right)$	-0.53	-1.60	-1.07

Table S3 Contributions to the enthalpy of solvation for TFE, EtOH and difference of these contributions for the two solutes.

Description	TFE (J/mol)	EtOH (J/mol)	EtOH - TFE (J/mol)
$\Delta E_{vib}^{libr}\left(\overline{\alpha_s^2}\right)$	345.97	1030.29	684.32
$\Delta E_{vib}^{tras}\left(\overline{\alpha_s^2}\right)$	22.23	66.27	44.04
$\Delta E_{vib}^{bend}\left(\overline{\alpha_s^2}\right)$	0.75	2.24	1.49
$\Delta E_{dist}\left(\overline{R}\right)$	-204.44	-388.34	-183.90
$\Delta E_s\left(\Delta\overline{R}\right)$	-206.09	-387.40	-181.31
$\Delta E_B\left(\overline{\alpha_s^2}\right)$	-752.91	-2244.88	-1491.97
$\Delta E_{rp}(T)$	0	0	0
ΔE_{el}	0	0	0

translational and bending distortions. ΔS_p is the proton disorder term, which is considered constant, as well as the non-bonded, long-range electrostatic energy E_{el}, while the E_{rp} is the temperature dependent, angle averaged radial potential describing the repulsive, dispersive and dipole–induced-dipole interactions between non bonded molecules. ΔE_{dist} is the molecular distortion induced by hydrogen bonds changing the zero point energies of intramolecular OH stretching modes, ΔS_R is the bond stretching configurational disorder, ΔE_s is the stretching energy perturbation, finally ΔS_B and ΔE_B are the configurational bending perturbation. All these thermodynamic quantities are reported per mole of solute, considering only the first solvation shell of EtOH and TFE relative to bulk water. When summed, these individual contributions reproduce the values listed in Tab. 2 of the main manuscript.

S2.7.3 Wrap water and HBhyd2bulk water distances trends

Fig. S9 illustrates how the distance cutoff used to define the wrap water affects the average O–O distances of the wrap water and the HBhyd2bulk hydrogen bond populations. The wrap water hydrogen bond population is defined as the layer of water molecules with oxygen within the given cutoff (r_{CH_3/F_3}) of the methyl or perfluoromethyl carbon, and which are hydrogen bonded to each other. The HBhyd2bulk hydrogen bond population is defined as the population of hydrogen bonds established between wrap

water molecules and those water molecules beyond the r_{CH_3/F_3} cutoff. The average O–O distances for (i) the wrap water hydrogen bond population, and (ii) the HBhyd2bulk hydrogen bond population are reported in Fig. S9. Within the investigated range of r_{CH_3/F_3} from 3.4 Å to 4.2 Å, the average O–O distance for the wrap water hydrogen bond population of EtOH (Fig. S9(i)) is consistently shorter than for bulk water, while for TFE the opposite is observed. For the HBhyd2bulk hydrogen bond population (Fig. S9(ii)), the average O–O distances for both solutes exceed those in bulk water, with TFE again showing larger values than EtOH. These trends are qualitatively independent of the chosen cutoff distance for defining the wrap water. Given their robustness, a cutoff of 3.66 Å from was used for the results reported in the main paper (Tab.4).

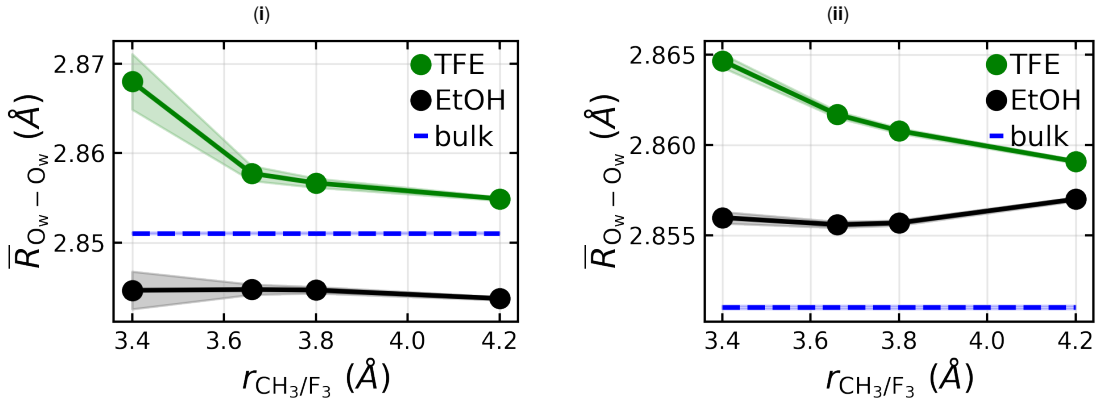

Fig. S9 Average O–O distances for (i) wrap water and (ii) HBhyd2bulk water, calculated using different cutoff definitions for the wrap water surrounding the methyl or perfluoromethyl groups. Data are shown for TFE (green), EtOH (black), and bulk water (dashed blue).

References

1 A. Perot and C. Fabry, On the application of interference phenomena to the solution of various problems of spectroscopy and metrology, *Astrophys. J.*, 1899, **9**, 87.

2 F. Neri, G. Saitta and S. Chiofalo, A simple procedure to remove the interference fringes from optical spectra, *J. Phys. E: Sci. Instrum.*, 1987, **20**, 894.

3 S. Burikov, T. Dolenko, S. Patsaeva, Y. Starokurov and V. Yuzhakov, Raman and IR Spectroscopy Research on Hydrogen Bonding in Water–Ethanol Systems, *Molecular Physics*, 2010, **108**, 2427–2436.

4 W. H. Press, *The art of scientific computing*, Cambridge Univ. Press, Cambridge [u.a.], 2nd edn, 1992.

5 L.-M. Liu, M. Krack and A. Michaelides, Interfacial water: A first principles molecular dynamics study of a nanoscale water film on salt, *J. Chem. Phys.*, 2009, **130**, 234702.

6 J. VandeVondele, F. Mohamed, M. Krack, J. Hutter, M. Sprik and M. Parrinello, The influence of temperature and density functional models in ab initio molecular dynamics simulation of liquid water, *J. Chem. Phys.*, 2004, **122**, 014515.

7 M. V. Fernández-Serra and E. Artacho, Network equilibration and first-principles liquid water, *J. Chem. Phys.*, 2004, **121**, 11136–11144.

8 J. R. Robalo, L. M. Streacker, D. Mendes de Oliveira, P. Imhof, D. Ben-Amotz and A. Vila Verde, Hydrophobic but water-friendly: Favorable water–perfluoromethyl interactions promote hydration shell defects, *J. Am. Chem. Soc.*, 2019, **141**, 15856–15868.

9 M. Heyden, J. Sun, S. Funkner, G. Mathias, H. Forbert, M. Havenith and D. Marx, Dissecting the THz spectrum of liquid water from first principles via correlations in time and space, *Proc. Natl. Acad. Sci. U.S.A.*, 2010, **107**, 12068–12073.

10 E. Schwegler, J. C. Grossman, F. Gygi and G. Galli, Towards an assessment of the accuracy of density functional theory for first principles simulations of water. II, *J. Chem. Phys.*, 2004, **121**, 5400–5409.

11 K. Forster-Tonigold and A. Groß, Dispersion corrected RPBE studies of liquid water, *J. Chem. Phys.*, 2014, **141**, 064501.

12 B. Madan and K. Sharp, Heat capacity changes accompanying hydrophobic and ionic solvation: A Monte Carlo and random network model study, *J. Phys. Chem.*, 1996, **100**, 7713–7721.

13 M. G. Sceats and S. A. Rice, The enthalpy and heat capacity of liquid water and the ice polymorphs from a random network model, *J. Chem. Phys.*, 1980, **72**, 3248–3259.

14 K. A. Sharp and B. Madan, Hydrophobic effect, water structure, and heat capacity changes, *J. Phys. Chem. B*, 1997, **101**, 4343–4348.

15 M. G. Sceats and S. A. Rice, The entropy of liquid water from the random network model, *J. Chem. Phys.*, 1980, **72**, 3260–3262.